RSC Advances

ROYAL SOCIETY OF CHEMISTRY

www.rsc.org/advances

Journal Name RSC Advances Dynamic Article Links ►

Cite this: DOI: 10.1039/c0xx00000x

www.rsc.org/xxxxxx

ARTICLE TYPE

Comparative investigation of microporous and nanosheet $LiVOPO_4$ as cathode materials for lithium-ion batteries

Jun-chao Zheng, Ya-dong Han, Bao Zhang *, Chao Shen, Lei Ming and Jia-feng Zhang*

# The authors (Jun-chao Zheng and Ya-dong Han) contributed equally to this work and should be considered co-first authors.

Received (in XXX, XXX) Xth XXXXXXXXX 20XX, Accepted Xth XXXXXXXXX 20XX

DOI: 10.1039/b000000x

$LiVOPO_4$ cathode materials are synthesized by freeze drying and spray drying methods. X-ray diffraction results reveal that the products obtained using the two methods are both in the β-$LiVOPO_4$ phase. SEM images demonstrate that the stacked nanosheets $LiVOPO_4$ were synthesized by freeze drying, whereas the microporous ones were synthesized by spray drying. Upon comparing the two methods, results indicate that the stacked nanosheets $LiVOPO_4$ synthesized by freeze drying exhibit much better electrochemical performance than microporous $LiVOPO_4$ synthesized by spray drying. The stacked nanosheets can deliver a capacity of 128.4 mAh g^{-1} at 0.1*C*, and possess favorable capacity at rates of 1*C* and 2*C*.

Introduction

The rapid development of lithium-ion batteries have overtaken that of the commercialized cathode material $LiCoO_2$, which is disadvantaged by its toxicity, the cost of cobalt, and the thermal stability[1, 2]. Considering the demand for rate capability, cycle life, safety, energy density, and environmental friendliness of cathode materials, transition-metal phosphates are attracting increased attention as a new class of cathode materials, including the commercialized $LiFePO_4$[3-5]. However, compared with $LiFePO_4$, β-$LiVOPO_4$ has a similar theoretical specific capacity (about 160 mAh g^{-1}) and higher charge–discharge potential (about 4.0V versus Li/Li^+) [6-8]. As an alternative cathode material, β-$LiVOPO_4$ is a promising cathode material for lithium batteries.

The main drawback of β-$LiVOPO_4$ is the poor electronic conductivity(about 10^{-10} S/cm)[6, 9-10] compared with other phosphate-based cathode materials, such as $LiFePO_4$[11, 12], $LiMnPO_4$[13, 14], $Li_3V_2(PO_4)_3$[15], and $LiVPO_4F$[16,17]. This poor conductivity affects the migration kinetics of Li^+ ions and electrons during the electrochemical reaction, influencing the rate performance. To solve these problems, numerous methods, such as carbothermal reduction method[6], sol-gel method[18], hydrothermal method[19, 20], etc., have been reported to synthesize $LiVOPO_4$. However, the conventional carbon coating faces a big bottle-neck to improve the electronic conductivity of $LiVOPO_4$, considering the material is synthesized in air atmosphere. Under such conditions, carbon is likely to burn out, leading to nearly no residue of the carbon component. Thus, there is not much improvement on electrochemical performances of $LiVOPO_4$ cathode material.

Therefore, exploring novel synthesis approaches is needed to overcome the above mentioned difficulties. Accordingly, we present here two novel methods (spray drying and freeze drying) to synthesize $LiVOPO_4$, with the properties investigated.

Experimental

First, A stoichiometric amount of NH_4VO_3 (AR, ≥99.0%), $NH_4H_2PO_4$ (AR, ≥99.0%), $LiNO_3$ (AR, ≥99.0%), and oxalic acid (AR, ≥99.0%) are mixed into deionized water with continuous stirring under 80 °C for 2 h, with the pH value of the solution adjusted to 7 using ammonia water. An orange cyan solution is then obtained. Second, the solution is transferred to the freeze dryer at –50 °C for 24 h in a vacuum with 15 Pa (or dried by a spray dryer with inlet temperature 260 °C) to obtain the $LiVOPO_4$ precursor. Finally, the precursor was sintered at 450 °C for 8 h in air atmosphere to obtain $LiVOPO_4$ samples.

The powder X-ray diffraction (XRD) (Rint-2000, Rigaku) measurement using Cu Kα radiation was employed to identify the crystalline phase of the synthesized materials. The valence state of vanadium in the prepared precursor was determined by an X-ray photoelectron spectrometer (XPS, KratosModel XSAM800) equipped with an Mg Kα achromatic X-ray source (1235.6 eV). The samples were observed with a JEOL, JSM-5600LV scanning electron microscopy (SEM) system and a Tecnai G12 transmission electron microscopy (TEM) system.

The electrochemical characterizations were performed using CR2025 coin-type cell. Typical positive electrode loadings were in the range of 2–2.5 mg/cm^2, and an electrode diameter of 14 mm was used. For positive electrode fabrication, the prepared powders were mixed with 10% of carbon black and 10% of polyvinylidene fluoride in N-methyl pyrrolidinone until slurry was obtained. Then, the blended slurries were pasted onto an aluminum current collector, and the electrode was dried at 120 °C for 12 h in argon. The test cell consisted of the positive electrode and lithium foil negative electrode separated by a porous polypropylene film, and 1 mol/L $LiPF_6$ in EC, EMC, and DMC (1:1:1 in volume) as the electrolyte. The assembly of the cells was carried out in a dry Ar-filled glove box. Electrochemical tests were carried out using an automatic galvanostatic charge–discharge unit, the NEWARE battery cycler. The cyclic

voltammetric measurements and EIS were carried out with a CHI660D electrochemical analyzer. The CV curves for the test cells were recorded in the potential range of 3.0–4.5 V. The impedance spectra were recorded by applying an AC voltage of 5 mV amplitude in the 100KHz–0.1 Hz frequency range.

Results and discussion

The XPS spectra of the $LiVOPO_4$ samples synthesized by spray drying and freeze drying are shown in Figs. 1(a) and (b), respectively. The binding energy (BE) values of V2p for the synthesized $LiVOPO_4$ are both approximately 517.1 and 524.8 eV, which correspond to energy level $V2p_{3/2}$ and $V2p_{1/2}$, respectively. Spin orbit coupling causes the V2p split [21]. The BE value of $V2p_{3/2}$ of the samples match well with values observed in VO_2 (517.1 eV) [22], indicating that the oxidation state of vanadium is +4.

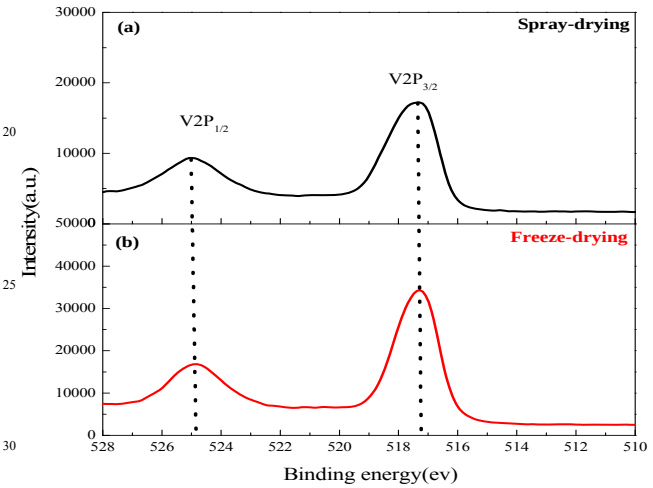

Fig. 1 XPS spectra of V2p of $LiVOPO_4$ synthesized by (a) spray drying and (b) freeze drying

Fig. 2(a) shows the XRD pattern of β-$LiVOPO_4$ synthesized by spray drying. As shown in the figure, all of the peaks can be indexed on the basis of the orthorhombic structure. The calculated lattice parameters of $LiVOPO_4$ are: a = 7.44363, b = 6.27918, c = 7.16752, α = β = γ = 90°, V = 334.9 $Å^3$ (shown in Table 1), which compares well with those reported by Barker et al. [6] (a = 7.446, b = 6.278, c = 7.165, α = β = γ = 90°).

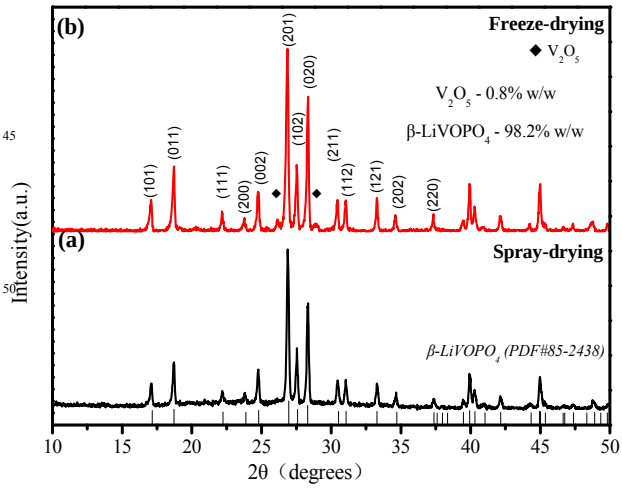

Fig. 2 XRD patterns of $LiVOPO_4$ synthesized by (a) spray drying and (b) freeze drying

Fig. 2(b) shows the XRD pattern of β-$LiVOPO_4$ synthesized by freeze drying. Two peaks at 26.1° and 28.9° are observed, which are ascribed to V_2O_5 impurity. The content of V_2O_5 is 0.8 wt%, determined by Rietveld analysis of XRD data. The calculated lattice parameters of $LiVOPO_4$ are: a = 7.46588, b = 6.2864, c = 7.17104, α = β = γ = 90°, V = 336.5$Å^3$ (shown in Table 1), which are slightly larger than that of the spray drying synthesized product, and that reported by Barker et al. [6].

Table 1 Refined unit cell lattice parameters for $LiVOPO_4$

Sample	a/Å	b/Å	c/Å	α	β	δ	V/$Å^3$
Freeze-drying	7.46588	6.2864	7.17104	90°	90°	90°	336.5
Spray-drying	7.44363	6.27918	7.16752	90°	90°	90°	334.9

The agreement factors are R_p (%) = 9.91 in $LiVOPO_4$ synthesized by freeze-drying; R_p (%) = 8.2 in $LiVOPO_4$ synthesized by spray-drying.

Figs. 3(a) and 3(b) presents the SEM and HRTEM images of the $LiVOPO_4$ samples synthesized by spray drying. Some micropores observably existed in the particles. The lattice fringe of $LiOVPO_4$ with an interplanar spacing of 0.33 nm corresponds to the (2 0 1) lattice planes in Fig. 3(f). Fig. 3(c) reveals the morphology of $LiVOPO_4$ powder synthesized by freeze drying. The $LiVOPO_4$ are notably built of nanosheets with thickness of about 100 nm (Fig. 3(d)). The nanosheets are stacked and agglomerated (Fig. 3(e)). Crystal planes with a d-spacing of 0.33 nm corresponds to the (2 0 1) planes of orthorhombic $LiVOPO_4$ in Fig.3(g), and no carbon coating layer is observed at the edge of the nanosheet.

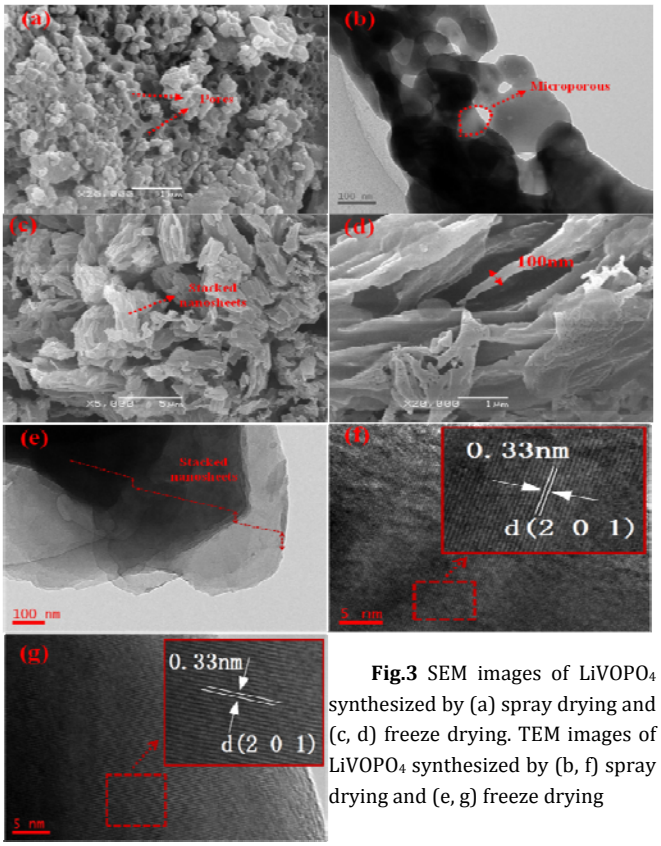

Fig.3 SEM images of $LiVOPO_4$ synthesized by (a) spray drying and (c, d) freeze drying. TEM images of $LiVOPO_4$ synthesized by (b, f) spray drying and (e, g) freeze drying

To the best of our knowledge, in a typical secondary battery, energy storage involves Faradaic reactions occurring at the surface of an electrode, and mass and charge transfer through the electrode; therefore, the surface area and the transport distance play important roles in determining the performance of the battery[23]. Many cathode materials face the polarization in the charger-discharger process, which influences the rate and cycle performance of cell[9, 13, 15-16]. The polarization is caused by slow lithium diffusion in the active material and increases in the resistance of the electrolyte when the charging–discharging rate is increased. To overcome these problems, it is important to design and fabricate nanostructured electrode materials that provide high surface area and short diffusion paths for ionic transport and electronic conduction[17]. The nanosheet morphology can offer improved energy storage capacity and charge–discharge kinetics, as well as better cyclic stabilities, owing to their large surface area for better contact between the active material and electrolyte which is better to the Faradaic reaction, and provide more sites for lithium ion intercalation and deintercalation; short distance for mass and charge diffusion which can allow for utilizing materials having low electronic conductivity; as well as the added freedom for volume change that accompanies lithium-ion charge and discharge[17,23,24]. Thus, the nanosheets should deliver good electrochemical performance.

Fig. 4.a–d show the charge–discharge curves of Li/$LiVOPO_4$ cells at different rates. The samples synthesized by freeze drying can notably deliver a capacity of 128.4, 100.9, 44, and 25.7 mAh g^{-1} at 0.1*C*, 0.2*C*, 1*C*, and 2*C*, respectively. However, the samples from spray drying only deliver 121.6, 94, 33.4, and 18.8 mAh g^{-1} at the corresponding rates. The polarization of samples synthesized by spray drying is much worse than that of freeze drying, especially at higher rates (1*C* and 2*C*). Fig.4e shows the cycling performance, which is not very good but is still better than that from other reports[6, 25]. The samples synthesized by freeze drying exhibit better cycle performance than that from spray drying. The better electrochemical performances of $LiVOPO_4$ synthesized by freeze drying may be attributed to the following reasons: First, the cell volume of $LiVOPO_4$ synthesized by freeze drying is larger than that by spray drying, which can provide a larger space for the movement of lithium ions and a smooth Li^+ diffusion tunnel in the charge–discharge process, thus, increase the Li^+ diffusion coefficient[26, 27]. Second, $LiVOPO_4$ with nanosheets structure synthesized by freeze drying can provide lithium ions with more sites, shorten diffusion distance, and maintain good contact between the active material and electrolyte.

Fig. 5 shows the cyclic voltammogram (CV) of β-$LiVOPO_4$ cathodes synthesized by spray drying and freeze drying, with Li-metals as the counter and reference electrode, in the potential range 3.0–4.5V at room temperature and a scan rate of 0.1 mV s^{-1}. It shows a typical CV of β-$LiVOPO_4$ cathode. The oxidation peak is located around 4.10 V and the reduction peak is located around 3.90 V for both electrodes, in agreement with the charge–discharge curves (Fig. 4. a–d). Some difference can be observed from the CV curves. First, the area bounded by the curve of β-$LiVOPO_4$ synthesized by freeze drying is bigger than that of spray drying, indicating the higher charge–discharge capacity. Second, after 50 cycles, the 1st, 2nd, and 50th curves of β-$LiVOPO_4$ electrode synthesized by freeze drying are almost the same, as shown in Fig. 5(b), indicating the small polarization and good cycling performance. The results are consistent with the charge–discharge curves and cycle performance.

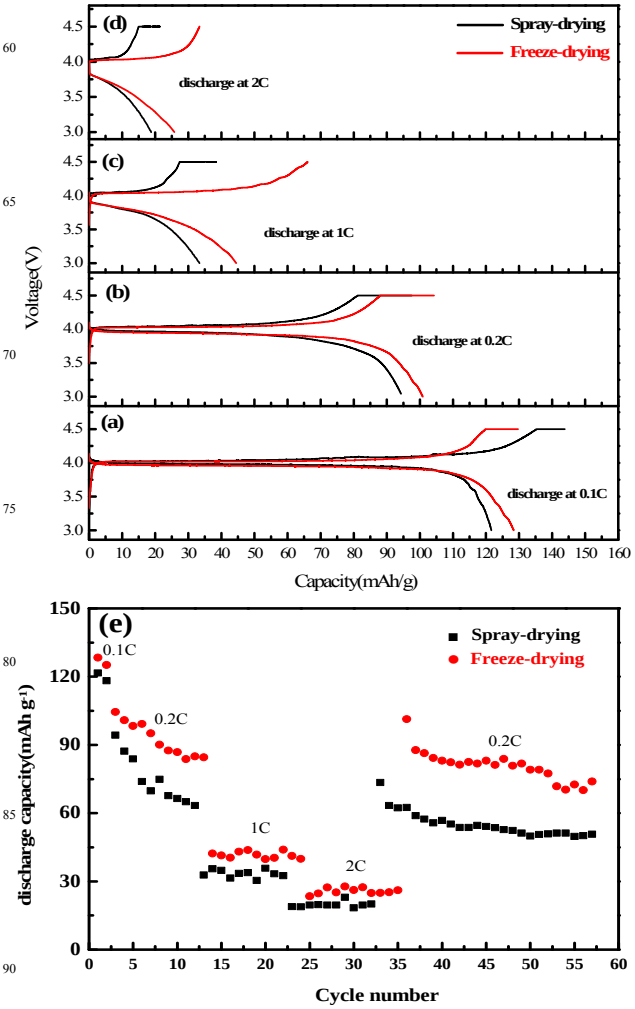

Fig. 4 Charge–discharge performance of $LiVOPO_4$ at (a) 0.1*C*, (b) 0.2*C*, (c) 1*C*, and (d) 2*C*,(e) Cycle performance of $LiVOPO_4$

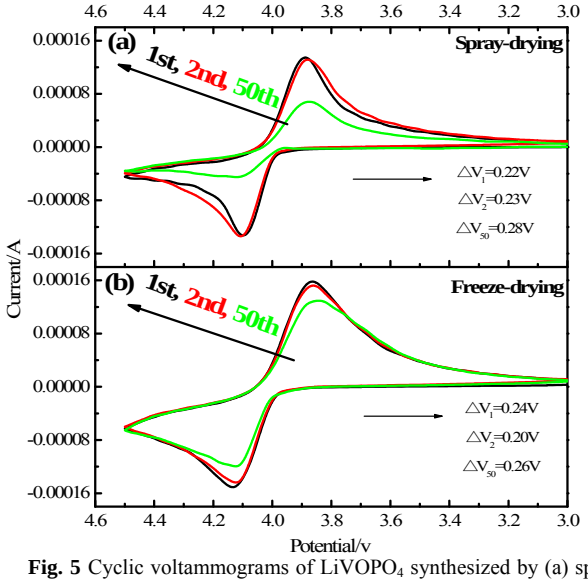

Fig. 5 Cyclic voltammograms of $LiVOPO_4$ synthesized by (a) spray drying and (b) freeze drying at a scan rate of 0.1 mV s^{-1}

Fig. 6(a) is the typical complex impedance spectra for the prepared $LiVOPO_4$. Both spectra show typical Nyquist characteristics. The solution resistance (Rs) is described by the intercept impedance in high frequency. The semicircle in the high-middle frequency region indicates the poor contact between current collector and active composite mass (Rct) [28, 29]. The line inclined in the low frequency region is associated with the Warburg impedance (Zw). Refinements of the diagrams were conducted by using the Zview program, and the equivalent circuit

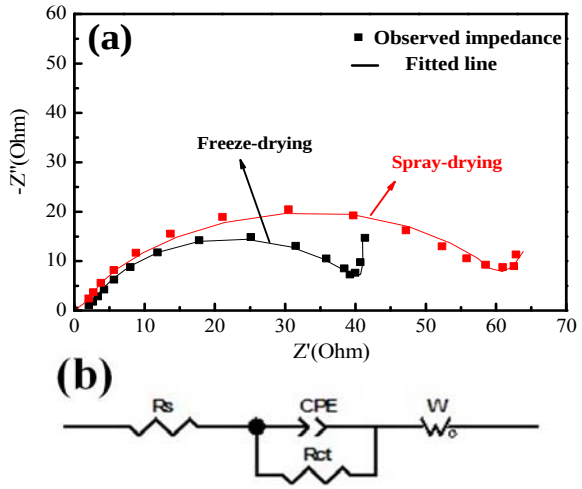

Fig. 6 (a) Electrochemical impedance spectra curves of $LiVOPO_4$ synthesized by spray drying and freeze drying. (b) Equivalent circuit used for fitting the experimental parameters of EIS

is shown in Fig. 6(b). The fit between the experimental data and equivalent circuit is very good. The parameters of the equivalent circuit are shown in Table 2. The Rct of $LiVOPO_4$ samples synthesized by freeze drying and spray drying are about 39.8 and 56.4 Ω, respectively. Consequently, lower resistance is more favorable for lithium insertion and de-insertion. Besides, the lower Warburg impedance (in Table.2) of samples synthesized by freeze drying indicates a fast Li^+ diffusion in $LiVOPO_4$ nanosheets. Therefore, the lower impedances of samples synthesized by freeze drying can obtain better electrochemical performance, which is consistent with the charge–discharge performance analysis above.

Table 2 The solution transfer resistance (R_s) and charge transfer resistance (R_{ct}) generated from the equivalent circuit fitting

Sample	Rs/Ω	Rct/Ω	CPE_b/μF	W/Ω
Freeze-drying	1.796	39.8	0.782	2.281
Spray-drying	1.981	56.4	0.773	22.32

Conclusions

The β-$LiVOPO_4$ cathode materials with stacked nanosheets and microporous morphology have been successfully synthesized by freeze-drying and spray-drying methods, respectively. The results indicate that the stacked nanosheets $LiVOPO_4$ synthesized by freeze drying exhibit much better electrochemical performance than that of spray drying, which is attributed to the structures and larger cell volumes of the nanosheets. Freeze drying is a novel way to improve the electrochemical performance of $LiVOPO_4$ by controlling its morphology.

Acknowledgment

This study was supported by National Natural Science Foundation of China (Grant No. 51302324 and 51272290).

Notes and references

1. S.B. Schougaard, J. Bréger and M. Jiang, Adv. Mater, 2006, 18, 905.
2. J. Cho and G. Kim, Electrochem. Solid-State Lett, 1999, 2, 253.
3. B. Scrosati and J. Garche, J. Power Sources, 2010, 195, 2419.
4. M. S. Whittingham, Chem.Rev, 2004,104, 4271.
5. J.W. Fergus, J. Power Sources, 2010, 195,939.
6. J. Barker and M.Y. Saidi, J. Electrochem. Soc, 2004, 15, A796.
7. B.M. Azmi and T. Ishihara, J. Power Sources, 2005, 146,525.
8. M.A. Bustam, S.M. Hasanaly and T. Ishihara, Ionics,2005, 11, 402.
9. C. J. Allen, Q. Jia and C. N. Chinnasamy, J. Electrochem. Soc, 2011, 158, A1250.
10. A.S. Hameed, M. Nagarathina and M.V. Reddy, J. Mater. Chem, 2012, 22, 7206.
11. A. Yamada, S.C. Chung and K. Hinokuma, J. Electrochem. Soc, 2001,148, A224.
12. R. Dominko, M. Bele and M. Gaberscek, J. Electrochem. Soc, 2005, 152, A607.
13. G. L, H. Azuma and M. Tohda, Electrochem. Solid-State Lett, 2002, 5, A135.
14. N. H. Kwon, T. Drezen and I. Exnar, Electrochem. Solid-State Lett, 2006, 9, A277.
15. A.P. Tang, X.Y. Wang and S.Y. Yang, J. Appl. Electrochem, 2008, 38 1453.
16. J. Barker, R.K.B. Gover and P. Burns, J. Power Sources, 2005, 146,516.
17. B. Zhang,Y. D.Han and J.C. Zheng, J. Power Sources, 2014, 264, 123.
18. A. Tang, J. Shen and Y.J. Hu, J. Electrochem. Soc. 2014,161, A10.
19. K. Saravanan and H.S. Lee, J. Mater. Chem, 2011, 21, 10042.
20. M. M. Ren, Z. Zhou and X. P. Gao, J. Phys. Chem.C,2008,112,13043.
21. M.V. Reddy, G.V. Subba Rao and B.V.R. Chowdari, J. Power Sources, 2010, 195, 5768.
22. J. Mendialdua and R. Casanova, Spectrosc. Relat.Phenom,1995, 71,249.
23. Y. Wang and G. Cao, Adv. Mater, 2008, 20,2251.
24. R. Pitchai, V. Thavasi and S. G. Mhaisalkar, J. Mater Chem, 2011, 21, 11040.
25. B.M. Azmi, H.S. Munira and T. shihara, Ionics, 2005, 11,402.
26. H. Liu, Q. Cao and L. J. Fu, Electrochem Commun, 2006, 8,1553.
27. H. Liu, C. Li and Q. Cao, J. Solid State Electrochem, 2008, 12, 1017.
28. M. Gaberscek, J. Moskon and B. Erjavec, Electrochem. Solid-State Lett, 2008, 11, A170.
29. J.M. Atebamba, J. Moskon and S. Pejovnik, J. Electrochemical. Soc, 2010, 157, A1218.